

# Direction-of-Arrival and Noise Covariance Matrix joint estimation for beamforming

Vitor G. P. Curtarelli<sup>✉</sup>, Stephan Paul<sup>✉</sup>, and Anderson W. Spengler<sup>✉</sup>

**Abstract**—We propose a joint estimation method for the Direction-of-Arrival (DoA) and the Noise Covariance Matrix (NCM), within the context of beamforming and signal enhancement. Building upon an existing NCM framework, our approach simplifies the NCM estimation procedure by deriving a quasi-linear solution, instead of the original exhaustive search. Additionally, we introduce a novel DoA estimation technique that operates across all frequency bins, improving robustness in reverberant environments and non-ideal scenarios. Simulation results demonstrate that our method outperforms classical techniques, such as MUSIC, achieving lower angular errors across a wide range of simulation conditions. The proposed framework was also fared against a MUSIC-based beamformer for signal enhancement, having similar overall noise rejection with superior interference canceling capabilities and desired-source maintenance.

**Index Terms**—Noise covariance matrix, direction of arrival estimation, signal enhancement, digital signal processing, array processing.

## I. INTRODUCTION

The employment of multi-sensor signal acquisition has become a cornerstone in modern signal processing, enabling more precise analysis and enhancing output quality across diverse domains [1]. Sensor array-based processing techniques find application in a wide range of scenarios, from assistive hearing devices [2] and smart home technologies [3], to radar systems [4], [5], wireless communications [6], [7], and biomedical instrumentation [8], [9]. In such settings, spatial filtering and signal enhancement are often essential, and hinge on accurate statistical models of the signal and its surrounding noise field. However, the effectiveness of such systems is highly dependent on accurate modeling and estimation processes. Among these, the estimation of signal characteristics — such as covariance structures and source positioning — plays a crucial role [10].

A key tool in this context is the signal’s covariance matrix (CM), which — in the present case — characterizes the

Manuscript Info: Corresponding author: Vitor G. P. Curtarelli.  
V. G. P. Curtarelli and A. W. Spengler are with the Electrical and Engineering Department at Universidade Federal de Santa Catarina (UFSC), Florianópolis, SC, Brazil (emails: vitor.curtarelli@posgrad.ufsc.br, anderson.spengler@ufsc.br).

S. Paul is with the Mechanical Engineering Department at Universidade Federal de Santa Catarina (UFSC), Florianópolis, SC, Brazil (email: stephan.paul@ufsc.br).

temporal-spatial relationships between received signals. While widely adopted, this approach can be severely affected by finite sample effects, noise, and rapidly changing environments and configurations [11]. In these cases, relying directly on the observed signal’s CM may result in suboptimal or biased signal enhancement performance [12].

An alternative lies in modeling the noise through a dedicated Noise Covariance Matrix (NCM) [13], [14], which separates desired from undesired components and provides a more robust foundation for tasks such as beamforming, interference suppression, and source separation [15], [16]. Nonetheless, estimating the NCM presents challenges — chiefly, the differentiation of signal and noisy sources, sensitivity to spatial correlations, and degradation under low-SNR conditions [11].

In many scenarios, NCM estimation is inherently linked to the estimation of the Direction-of-Arrival (DoA) of one or more interfering sources [5], [17]. However, traditional DoA estimation methods often rely on exhaustive search techniques, which are computationally expensive and sensitive to initial conditions [18], [19].

In this work, we propose a novel method for jointly estimating the NCM of a contaminated sound field and the DoA of a directional interfering source. Building upon the NCM modeling approach in [20], our method introduces a broadband cost function which extends the model to also include the estimation of an interfering source’s DoA, along with an improved mathematical optimization framework that allows for quasi-linear estimation of the modeled signals’ variances. This leads to a significant reduction in computational complexity while maintaining (or even improving) estimation accuracy and filtering performance.

Importantly, our results show that the proposed DoA estimator outperforms traditional approaches such as MUSIC both in accuracy and precision, while enabling more effective beamforming when integrated into a full signal enhancement pipeline. These results are validated across almost 1500 combinations of acoustic parameters, such as varying input SNR values, reverberation times, and source positions.

## II. SIGNAL MODEL

We consider a generic sensor array comprised of  $M$  omnidirectional sensors within a reverberant environment, populated by both desired and contaminating sources. We assume this environment to be stationary both spatially and for its statistical characteristics; these constraints are primarily for ease of notation and algebra, being easily removable for a more general case or practical applications.

In the time domain, the observed signal at the  $m$ -th sensor is  $y_m(t)$ , and is modeled as

$$y_m(t) = s_m(t) + n_m(t) + \sum_{i=1}^I w_{m,i}(t) + v_m(t), \quad (1)$$

where:  $s_m(t)$  is the reverberant desired signal;  $n_m(t)$  and  $w_{m,i}(t)$  are undesired signals, with  $n_m(t)$  being the dominant among these (which will be called interfering signal), and  $w_{m,i}(t)$  originating from other (less impactful) undesired sources; and  $v_m(t)$  is uncorrelated Gaussian noise modeling thermal noise. These signals all refer to the  $m$ -th sensor within the sensor array.

Transforming all signals into the (discrete) time-frequency domain (with  $l$  representing the time-frequency window index, and  $k$  the frequency bin), and decomposing the reverberant desired and interfering signals into a sum of planar waves [20], we have the modeled observed signal  $\hat{y}_m[l, k]$

$$\begin{aligned} \hat{y}_m[l, k] &\approx y_m[l, k] \\ &= \sum_{j_s=1}^{J_s} s_{m,j_s}[l, k] + \sum_{j_p=1}^{J_p} n_{m,j_p}[l, k] \\ &\quad + \sum_{i=1}^I w_{m,i}[l, k] + v_m[l, k], \end{aligned} \quad (2)$$

where  $\hat{y}_m[l, k]$  is the approximate model of  $y_m[l, k]$ , under the presented assumptions. Through the text, the tilde accent will denote a model or approximation for the accented variable.

Now, three modeling assumptions are taken:

- 1) Each planar wave decomposition is dominated by a single plane-wave [21] ( $j_s = j_p = 1$ ), and this is the direct-path between the source and the  $m$ -th sensor;
- 2) This direct-path component can be written in terms of the relative frequency response (RFR) between the reference ( $m = 1$ ) and the  $m$ -th sensors;
- 3) All non-direct-path components of  $s_m[l, k]$  and  $n_m[l, k]$  ( $j_s \geq 2$  and  $j_p \geq 2$ ), and all non-dominant undesired sources  $w_{m,i}[l, k]$ , can be packed into a single variable  $\gamma_m[l, k]$ .

With these, we can write the modeled signal  $\hat{y}_m[l, k]$  as

$$\hat{y}_m[l, k] = d_m[k]x_1[l, k] + b_m[k]p_1[l, k] + \gamma_m[l, k] + v_m[l, k]. \quad (3)$$

in which:  $x_1[l, k]$  and  $p_1[l, k]$  are (respectively) the desired and interfering signal's first planar-wave at the reference sensor;  $\gamma_m[l, k]$  is the previously defined contaminating signal,

$$\gamma_m[l, k] = \sum_{j_s=2}^{J_s} s_{m,j_s}[l, k] + \sum_{j_p=2}^{J_p} n_{m,j_p}[l, k] + \sum_{i=1}^I w_{m,i}[l, k]; \quad (4)$$

and  $d_m[k]$  and  $b_m[k]$  are (respectively) the desired and interfering signal's reference-to- $m$ -th RFRs, given by

$$d_m[k] = e^{-j2\pi \frac{k f_0}{K \cdot c} r_m \cos(\theta_d - \psi_m) \cos(\phi_d - \lambda_m)}, \quad (5a)$$

$$b_m[k] = e^{-j2\pi \frac{k f_0}{K \cdot c} r_m \cos(\theta_b - \psi_m) \cos(\phi_b - \lambda_m)}, \quad (5b)$$

with  $e$  denoting the Neperian constant. Here,  $f_0$  is the sampling frequency,  $K$  is the total number of frequency bins,  $c = 343\text{m/s}$  is the wave speed,  $(r_m, \psi_m, \lambda_m)$  are the spherical coordinates of the  $m$ -th sensor (distance, azimuth, elevation), and  $(\theta_d, \phi_d)$  is the desired source's angular direction; equivalently for  $(\theta_b, \phi_b)$  as the interfering source's angular direction. All these spherical measurements are assuming the reference sensor as the origin.

Finally, we define  $\tilde{\mathbf{y}}[l, k] = [\hat{y}_1[l, k], \dots, \hat{y}_M[l, k]]^\top$  as the column vectorization of the modeled observed signals, and  $\mathbf{d}[k], \mathbf{b}[k], \boldsymbol{\gamma}[l, k]$  and  $\mathbf{v}[l, k]$  are defined similarly; with  $(\cdot)^\top$  being the transpose operator. Our sensor-stacked modeled observed signal can alternatively be written as

$$\tilde{\mathbf{y}}[l, k] = \mathbf{d}[k]x_1[l, k] + \mathbf{b}[k]p_1[l, k] + \boldsymbol{\gamma}[l, k] + \mathbf{v}[l, k]. \quad (6)$$

We let  $\boldsymbol{\eta}$  be the modeled global noise vector encompassing all non-desired signals, such that

$$\tilde{\mathbf{y}}[l, k] = \mathbf{b}[k]p_1[l, k] + \boldsymbol{\gamma}[l, k] + \mathbf{v}[l, k], \quad (7)$$

with which

$$\tilde{\mathbf{y}}[l, k] = \mathbf{d}[k]x_1[l, k] + \tilde{\boldsymbol{\eta}}[l, k]. \quad (8)$$

An example of a considered environment layout is in Fig. 1, with desired and contaminating sources, considering their direct and reflecting paths.

### A. Observed signal covariance matrix modeling

We write the observed signal's covariance matrix as  $\mathbf{R}_y[k]$ , and it is given by

$$\mathbf{R}_y[k] = \mathbb{E}_l \left\{ \mathbf{y}[l, k] \mathbf{y}^\text{H}[l, k] \right\}, \quad (9)$$

in which  $\{\cdot\}^\text{H}$  represents the conjugate-transpose operation, and  $\mathbb{E}\{\cdot\}$  is the expectation operator — in this case, with respect to the window index  $l$ . We also define  $\mathbf{R}_{\tilde{\mathbf{y}}}[k]$  as the modeled observed signal's CM, which — given Eq. (6) — can be expanded to

$$\mathbf{R}_{\tilde{\mathbf{y}}} = \bar{\mathbf{R}}_x \sigma_{x_1}^2 + \bar{\mathbf{R}}_p \sigma_{p_1}^2 + \bar{\mathbf{R}}_\gamma \sigma_{\gamma_1}^2 + \bar{\mathbf{R}}_v \sigma_{v_1}^2 + \epsilon \mathbf{I}, \quad (10)$$

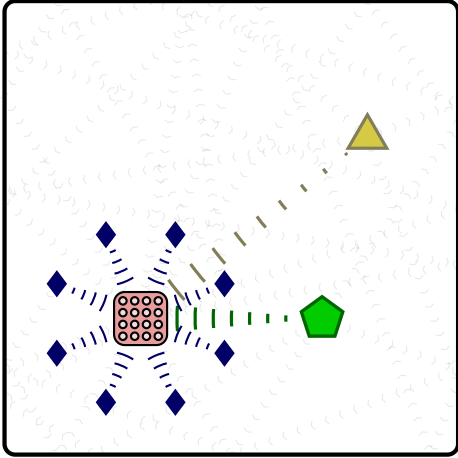


Fig. 1: Example of room layout, with: desired (green pentagon), interfering (yellow triangle), and correlated (blue diamond) sources; direct-path (opaque, with the color of the respective source) and reverberations (translucent gray arrows); and a sensor array (red rectangle), with sensors represented by small circles.

where  $\sigma_{x_1}^2[k]$  is the variance of  $x_1[l, k]$  and  $\bar{\mathbf{R}}_x[k] = (\mathbf{d}\mathbf{d}^H)[k]$  is its pseudo-normalized covariance matrix (these being denoted by the bar); and similarly for  $\sigma_{p_1}^2[k]$ ,  $\sigma_{\gamma_1}^2[k]$  and  $\sigma_{v_1}^2[k]$ , as well as  $\bar{\mathbf{R}}_p[k] = (\mathbf{b}\mathbf{b}^H)[k]$ ,  $\bar{\mathbf{R}}_\gamma[k]$  and  $\bar{\mathbf{R}}_v[k]$ .  $\epsilon$  is a normalization factor, to ensure a minimal white noise presence on the modeled matrix.  $\bar{\mathbf{R}}_x[k]$  is implicitly a function of  $\Theta_d = (\theta_d, \phi_d)$ , and so is  $\bar{\mathbf{R}}_p[k]$  (a function) of  $\Theta_b = (\theta_b, \phi_b)$ . While not explicit in Eq. (10), all covariance matrices and variances (except  $\epsilon$ ) are bin dependent, but not window dependent, due to the stationarity assumptions.

Now, some modeling assumptions are made:

- 1) The desired source's direction, as well as  $\mathbf{d}[l, k]$ , are known;
- 2)  $\mathbf{v}[l, k]$  is spatially uncorrelated Gaussian noise, such that  $\bar{\mathbf{R}}_v[l, k] = \mathbf{I}$ ;
- 3)  $\gamma[l, k]$  is a spherically isotropic noise [20], and thus  $\bar{\mathbf{R}}_\gamma[l, k]$  is known [22];
- 4) The DoA  $\Theta_b$ , which dictates  $\mathbf{b}[l, k]$ , is constant across the frequency spectrum.

Although we take all (except  $\bar{\mathbf{R}}_p[k]$ ) covariance matrices to be known, their respective variances are not. Therefore, we have  $4K+2$  unknown in our problem: for each frequency, the variances for all signals at the reference sensor,  $\sigma_{x_1}^2$ ,  $\sigma_{u_1}^2$ ,  $\sigma_{\gamma_1}^2$  and  $\sigma_{v_1}^2$ ; and the DoA  $\Theta_b$  which dictates the steering vector for the interfering signal.

Assuming the knowledge of these variances and of  $\Theta_b$ , the global noise covariance matrix  $\mathbf{R}_\eta[k]$  can be estimated as  $\bar{\mathbf{R}}_\eta[k]$ , which through the definition of  $\tilde{\eta}[l, k]$  in Eq. (7) can be written as

$$\mathbf{R}_{\tilde{\eta}} = \bar{\mathbf{R}}_p \sigma_{p_1}^2 + \bar{\mathbf{R}}_\gamma \sigma_{\gamma_1}^2 + \bar{\mathbf{R}}_v \sigma_{v_1}^2 + \epsilon \mathbf{I}. \quad (11)$$

We highlight that  $\mathbf{R}_{\tilde{\eta}} \equiv \mathbf{R}_{\tilde{\eta}}[k]$  is frequency-dependent (similarly to all other covariance matrices), this being omitted in Eq. (11) to save space. Note the  $\epsilon \mathbf{I}$ , added to force a minimal white noise consideration.

### III. DOA AND NCM ESTIMATION

Given the desire to find the most appropriate values for the DoA  $\Theta_b$  and for the variances, a minimization scheme must be carefully constructed.

We define  $\boldsymbol{\sigma}_k[k] = [\sigma_{x_1}^2[k], \sigma_{p_1}^2[k], \sigma_{\gamma_1}^2[k], \sigma_{v_1}^2[k]]$  as a vector of the unknown variances, and  $F(\bar{\mathbf{R}}_{\tilde{\eta}}(\boldsymbol{\sigma}_k, \Theta_b)[k])$  as a frequency-dependent cost function, given by the  $l_2$  norm

$$F(\bar{\mathbf{R}}_{\tilde{\eta}}(\boldsymbol{\sigma}_k, \Theta_b))[k] = \|\bar{\mathbf{R}}_{\tilde{\eta}}[k] - \mathbf{R}_y[k]\|_2^2, \quad (12)$$

where this cost function is implicitly dependent on  $\Theta_b$  and  $\boldsymbol{\sigma}_k$ , as well as on the frequency bin  $k$ . We denote  $R_{z,j}$  as the  $j$ -th element of a generic  $\mathbf{R}_z$  ( $j = [i, j]$ ). With this, the cost function can be expanded to

$$F(\bar{\mathbf{R}}_{\tilde{\eta}}(\boldsymbol{\sigma}_k, \Theta_b))[k] = \sum_j \left| \left[ \sum_{z \in \mathcal{S}[k]} \bar{R}_{z,j}[k] \sigma_{z_1}^2[k] \right] - (R_{y,j}[k] - \epsilon I_j) \right|^2, \quad (13)$$

with  $\mathcal{S}[k] = \{\mathbf{x}[k], \mathbf{p}[k], \boldsymbol{\gamma}[k], \mathbf{v}[k]\}$ . For notation, we let  $\mathbf{R}_{y,\epsilon} \equiv \mathbf{R}_y - \epsilon \mathbf{I}$ .

By splitting the absolute value's calculation into the squared sum of real and imaginary components, Eq. (13) can be modified into Eq. (14), where the superscripts  $\mathbb{R}$  and  $\mathbb{I}$  indicate the real and imaginary parts of the value, respectively.

$$\begin{aligned} F(\bar{\mathbf{R}}_{\tilde{\eta}}(\boldsymbol{\sigma}_k, \Theta_b))[k] &= \sum_j \left( \left[ \sum_{z \in \mathcal{S}[k]} \bar{R}_{z,j}^{\mathbb{R}}[k] \sigma_{z_1}^2[k] \right] - R_{y,\epsilon,j}^{\mathbb{R}}[k] \right)^2 \\ &\quad + \sum_j \left( \left[ \sum_{z \in \mathcal{S}[k]} \bar{R}_{z,j}^{\mathbb{I}}[k] \sigma_{z_1}^2[k] \right] - R_{y,\epsilon,j}^{\mathbb{I}}[k] \right)^2. \end{aligned} \quad (14)$$

Given the frequency-dependent cost function  $F(\bar{\mathbf{R}}_{\tilde{\eta}}(\boldsymbol{\sigma}_k, \Theta_b))[k]$ , we now define our broadband cost function  $\mathcal{F}(\boldsymbol{\Sigma}, \Theta_b)$  as the spectrum sum of the frequency-dependent one,

$$\mathcal{F}(\boldsymbol{\Sigma}, \Theta_b) = \sum_k F(\bar{\mathbf{R}}_{\tilde{\eta}}(\boldsymbol{\sigma}_k, \Theta_b))[k], \quad (15)$$

$\boldsymbol{\Sigma}$  containing the  $4K$  variances for all frequency bins.

#### A. Minimization on variances

Physically, the variances must be strictly non-negative, and therefore a minimization problem would need to satisfy this condition; that is,  $\boldsymbol{\sigma}_k \geq \mathbf{0} \ \forall k$ . The subspace of  $\mathbb{R}^4$  defined

by this constraint will be called the *feasible region*. An approach similar to the Lagrangian multiplier method [23] will be employed to approach this problem, inserting the constraints into the minimization function. For such, we define the Lagrangian function  $\mathcal{L}(\Sigma, \Theta_b, \zeta, \mu)$  as

$$\mathcal{L}(\Sigma, \Theta_b, \zeta, \mu) = \mathcal{F}(\Sigma, \Theta_b) - \zeta^\top(\sigma_k - \mu), \quad (16)$$

with  $\mu = [\mu_x^2, \mu_p^2, \mu_\gamma^2, \mu_v^2]$  being slack variables (given the inequality constraint), and  $\zeta$  being the Lagrangian multiplier vector, both implicitly frequency-dependent. We denote  $(\Sigma^*, \Theta_b^*, \zeta^*, \mu^*)$  as the optimal solution that minimizes the Lagrangian, namely

$$\Sigma^*, \Theta_b^*, \zeta^*, \mu^* = \underset{\Sigma, \Theta_b, \zeta, \mu}{\operatorname{argmin}} \mathcal{L}(\Sigma, \Theta_b, \zeta, \mu). \quad (17)$$

Since  $F(\mathbf{R}_y(\sigma_k, \Theta_b))[k]$  for each frequency bin is independent from another bin in terms of their variances, taking the derivative of the Lagrangian w.r.t. (with respect to) any variance  $\sigma_{z_1}^2[k]$  yields

$$\frac{\partial \mathcal{L}}{\partial \sigma_{z_1}^2[k]} = \sum_{\mathbf{w} \in S[k]} A_{\mathbf{w};\mathbf{z}}[k] \sigma_w^2[k] - A_{\mathbf{y},\epsilon;\mathbf{z}}[k] - \zeta_z[k], \quad (18)$$

where  $A_{\mathbf{w};\mathbf{z}}$  is

$$A_{\mathbf{w};\mathbf{z}}[k] = 2 \sum_{\mathbf{j}} \bar{R}_{\mathbf{w};\mathbf{j}}^{\mathbb{R}}[k] \bar{R}_{\mathbf{z};\mathbf{j}}^{\mathbb{R}}[k] + \bar{R}_{\mathbf{w};\mathbf{j}}^{\mathbb{I}}[k] \bar{R}_{\mathbf{z};\mathbf{j}}^{\mathbb{I}}[k], \quad (19)$$

also acting as a placeholder variable. The derivative in Eq. (18) can be straightforwardly obtained from Eq. (14). Note that these derivatives are taken regarding  $\sigma_{z_1}^2[k]$  and not  $\sigma_{z_1}[k]$ , as the latter would result in a cubic problem instead of a linear one, for which the direct solutions would be  $\Sigma = \mathbf{0}$  (corresponding to a local maximum), and the solution to deriving w.r.t.  $\sigma_{z_1}^2[k]$ .

Differentiating the Lagrangian w.r.t.  $\zeta_z[k]$  and  $\mu_z[k]$  yields respectively

$$\frac{\partial \mathcal{L}}{\partial \zeta_z[k]} = \sigma_{z_1}^2[k] - \mu_z[k], \quad (20a)$$

$$\frac{\partial \mathcal{L}}{\partial \mu_z[k]} = 2\zeta_z\mu_z. \quad (20b)$$

The variances vector which minimizes the cost function from Eq. (15) is one of the solutions where all derivatives in Eqs. (18), (20a) and (20b) are zero. To find the physically meaningful solution (within the feasible region  $\Sigma \geq \mathbf{0}$ ), first we will solve the unconstrained variance minimization problem, then use this solution to achieve the optimal variance vector for the constrained problem.

### 1) Unconstrained solution

Since the Lagrangian w.r.t. any variance depends only on the variances in its own frequency bin (Eq. (18)), our global minimization problem over all  $4K$  variances becomes  $K$  independent problems each with 4 variables, and for each  $k$  the (unconstrained) minimization can be written as

$$\mathbf{A}[k]\sigma_k = \mathbf{q}[k], \quad (21)$$

---

### Algorithm 1 Active-inactive constraints analysis

---

```

1:  $\sigma^* \leftarrow \underset{\sigma}{\operatorname{argmin}} F(\sigma)$ 
2:  $S \leftarrow \{\sigma^* < 0\}$  #  $\sigma^*$  negative entry indices set
3: for  $n = 1, \dots, |\{\sigma^* < 0\}|$  do
4:   for  $c \in \mathbf{P}_n(S)$  do
    #  $\mathbf{P}_n(S)$  is all  $n$ -element sets in the power-set of  $S$ 
    #  $c$  is a combination with  $n$  active constraints
5:      $\sigma^* \leftarrow \underset{\sigma}{\operatorname{argmin}} F(\sigma)$  with active  $c$ -th constraints
6:    $\sigma^\dagger \leftarrow \sigma$  if  $F(\sigma) < F(\sigma^\dagger)$ 
7: end for
8: break if  $\sigma^\dagger \geq 0$ 
9: end for

```

---

where

$$\mathbf{A}[k] = \begin{bmatrix} A_{\mathbf{x};\mathbf{x}}[k] & A_{\mathbf{p};\mathbf{x}}[k] & A_{\mathbf{y};\mathbf{x}}[k] & A_{\mathbf{v};\mathbf{x}}[k] \\ A_{\mathbf{x};\mathbf{p}}[k] & A_{\mathbf{p};\mathbf{p}}[k] & A_{\mathbf{y};\mathbf{p}}[k] & A_{\mathbf{v};\mathbf{p}}[k] \\ A_{\mathbf{x};\mathbf{y}}[k] & A_{\mathbf{p};\mathbf{y}}[k] & A_{\mathbf{y};\mathbf{y}}[k] & A_{\mathbf{v};\mathbf{y}}[k] \\ A_{\mathbf{x};\mathbf{v}}[k] & A_{\mathbf{p};\mathbf{v}}[k] & A_{\mathbf{y};\mathbf{v}}[k] & A_{\mathbf{v};\mathbf{v}}[k] \end{bmatrix}, \quad (22a)$$

$$\mathbf{q}[k] = \begin{bmatrix} A_{\mathbf{y},\epsilon;\mathbf{x}}[k] + \zeta_x[k] \\ A_{\mathbf{y},\epsilon;\mathbf{p}}[k] + \zeta_u[k] \\ A_{\mathbf{y},\epsilon;\mathbf{y}}[k] + \zeta_\gamma[k] \\ A_{\mathbf{y},\epsilon;\mathbf{v}}[k] + \zeta_v[k] \end{bmatrix}. \quad (22b)$$

Reasonably assuming  $\mathbf{A}[k]$  to be a full-rank matrix, the solution to the unconstrained problem is

$$\sigma_k^*[k] = \mathbf{A}^{-1}[k]\mathbf{q}[k]. \quad (23)$$

This result doesn't necessarily respect the constraint  $\sigma_k \geq 0$ , as neither of the variables  $\mathbf{A}^{-1}[k]$  or  $\mathbf{q}[k]$  — nor their product — are guaranteed to be positive.

### 2) Constrained solution

For each of the signals (generically  $z[l, k]$ ), from Eq. (20b) we have two options: either  $\zeta_z[k] = 0$ , meaning the constraint is inactive and the minimization is unrestricted in  $z$ ; or  $\mu_z[k] = 0$ , which from setting Eq. (20a) implies that  $\sigma_{z_1}^2[k] = 0$ , meaning the constraint is active. The unconstrained problem's process can be adapted to find the restricted problem's solution by following Algorithm 1; with all related proofs for its application in Theorems 1 and 2, from appendix A.

Note that the  $z$ -th constraint being active implies  $\sigma_{z_1}^2 = 0$ , removing its respective element from  $\sigma$  and  $\mathbf{q}[k]$ , and rows and column from  $\mathbf{A}[k]$ . Thus, at most  $2^4 = 16$  matrix inversions are sufficient to achieve the optimal constraint solution, with the worst case being with  $\sigma^\dagger = \mathbf{0}$ . We say that a quasi-linear solution to the variances minimization can be achieved, not relying on iterative processes. This active-inactive constraints analysis is repeated for all  $k$  frequency bins, achieving the  $4K$  solutions for the variances.

### B. Minimization on DoA

The previously minimization scheme solved only for  $\Sigma$ , treating  $\Theta_b$  as a constant. Since any element of  $\mathbf{A}[k]$  and  $\mathbf{q}[k]$  that corresponds to  $\mathbf{p}[k]$  depends on  $\Theta_b$ , so do the achieved solutions. That is, for each direction  $\Theta_b$ , we can find a solution on  $\Sigma$  which minimizes the error between  $\mathbf{R}_{\bar{\mathbf{y}}}[k]$  and  $\mathbf{R}_{\mathbf{y}}[k]$ , within the feasible region defined by the positive-variance constraints; but this achieved solution isn't necessarily a global minimum, being necessary a minimization on  $\Theta_b$ .

By definition,  $\bar{R}_{\mathbf{p};\mathbf{j}}(\Theta_b, \phi_b)$  depends on the relative (spherical) position between sensors  $i$  and  $j$  ( $\mathbf{j} = [i, j]$ ), and can be written as

$$\bar{R}_{\mathbf{p};\mathbf{j}}(\Theta_b, \phi_b) = e^{-j \frac{2\pi k f_0}{K_c} r_{\mathbf{j}} \cos(\Theta_b - \psi_{\mathbf{j}}) \cos(\phi_b - \lambda_{\mathbf{j}})}, \quad (24)$$

where  $r_{\mathbf{j}}$ ,  $\psi_{\mathbf{j}}$  and  $\lambda_{\mathbf{j}}$  are the relative spherical coordinates (distance, azimuth, and elevation) between the  $i$ -th and  $j$ -th sensors.

Since the Lagrangian constraints term  $\zeta^T(\sigma_k - \mu)$  doesn't depend on any of  $\theta_b$  or  $\phi_b$ , the Lagrangian's (Eq. (16)) derivatives w.r.t.  $\theta_b$  and  $\phi_b$  are, respectively,

$$\frac{\partial \mathcal{L}}{\partial \theta_b} = -\frac{4\pi f_0}{K_c} \sum_{\mathbf{j}} f_{1;\mathbf{j}}(\theta_b, \phi_b) G_{\mathbf{j}}(\theta_b, \phi_b), \quad (25)$$

$$\frac{\partial \mathcal{L}}{\partial \phi_b} = -\frac{4\pi f_0}{K_c} \sum_{\mathbf{j}} f_{2;\mathbf{j}}(\theta_b, \phi_b) G_{\mathbf{j}}(\theta_b, \phi_b), \quad (26)$$

with

$$f_{1;\mathbf{j}}(\theta_b, \phi_b) = \sin(\theta_b - \psi_{\mathbf{j}}) \cos(\phi_b - \lambda_{\mathbf{j}}), \quad (27a)$$

$$f_{2;\mathbf{j}}(\theta_b, \phi_b) = \cos(\theta_b - \psi_{\mathbf{j}}) \sin(\phi_b - \lambda_{\mathbf{j}}), \quad (27b)$$

$$G_{\mathbf{j}}(\theta_b, \phi_b) = r_{\mathbf{j}} \sum_k k \sigma_{p1}^2[k] \left\{ \hat{R}_{\mathbf{j}}^*[k] \bar{R}_{\mathbf{p};\mathbf{j}}(\theta_b, \phi_b)[k] \right\}^{\mathbb{I}}, \quad (27c)$$

where  $\hat{R}_{\mathbf{j}}[k]$  is the  $\mathbf{j}$ -th element of  $(\mathbf{R}_{\bar{\mathbf{y}}}[k] - \mathbf{R}_{\mathbf{y},\epsilon}[k])$ , and  $[\cdot]^*$  denotes the complex conjugate operation. Moving forward the  $4\pi f_0/c$  term will be ignored, given it is a positive constant. We also consider the following:

- For any diagonal element,  $r_{[i,i]} = 0$ ;
- For any element  $-\mathbf{j} \equiv [j, i]$ :
  - $r_{-\mathbf{j}} = r_{\mathbf{j}}$
  - $\psi_{-\mathbf{j}} = \psi_{\mathbf{j}} + \pi$
  - $\lambda_{-\mathbf{j}} = -\lambda_{\mathbf{j}}$
  - $G(\theta_b, \phi_b, -\mathbf{j}) = -G_{\mathbf{j}}(\theta_b, \phi_b)$

With these properties, we have that

$$f_1(\theta_b, \phi_b, -\mathbf{j}) = -\sin(\theta_b - \psi_{\mathbf{j}}) \cos(\phi_b + \lambda_{\mathbf{j}}), \quad (28a)$$

$$f_2(\theta_b, \phi_b, -\mathbf{j}) = -\cos(\theta_b - \psi_{\mathbf{j}}) \sin(\phi_b + \lambda_{\mathbf{j}}). \quad (28b)$$

By gathering the  $\mathbf{j}$  and  $-\mathbf{j}$  terms in the summations of Eqs. (25) and (26), through trigonometric properties they can be simplified to

$$\frac{\partial \mathcal{L}}{\partial \theta_b} = 2 \cos(\phi_b) \sum_{\substack{\mathbf{j}=[i,j] \\ i < j}} \sin(\theta_b - \psi_{\mathbf{j}}) \cos(\lambda_{\mathbf{j}}) G_{\mathbf{j}}(\theta_b, \phi_b), \quad (29a)$$

$$\frac{\partial \mathcal{L}}{\partial \phi_b} = 2 \sin(\phi_b) \sum_{\substack{\mathbf{j}=[i,j] \\ i < j}} \cos(\theta_b - \psi_{\mathbf{j}}) \cos(\lambda_{\mathbf{j}}) G_{\mathbf{j}}(\theta_b, \phi_b). \quad (29b)$$

Both  $\frac{\partial \mathcal{L}}{\partial \theta_b}$  and  $\frac{\partial \mathcal{L}}{\partial \phi_b}$  are heavily non-linear, and therefore a direct/linear solution isn't available. However, as this is an unconstrained minimization problem with restricted domain, an arbitrarily accurate solution can be achieved through methods such as iterative minimization or exhaustive search.

We propose the use of the gradient descent technique, as both the cost function and its derivatives are available. Since it requires an initial guess, our minimization process can either use a multi-initialization step, or a previously estimated DoA for configurations and sources which aren't spatially and statistically stationary.

### C. Approximations and specific-array considerations

Although the established process is generic and works with any sensor configuration, simplifications and approximations can be explored, for the general case and for specific scenarios.

#### 1) General approximation

From Eq. (29), it is easy to see that  $\phi_b = \pm 90^\circ$  leads to a null in  $\partial \mathcal{L} / \partial \theta_b$ , and  $\phi_b = 0^\circ$  a null in  $\partial \mathcal{L} / \partial \phi_b$ . However, these nulls are due to the geometric construction and choice of variables, and unrelated to the DoA estimation procedure. They are also linked to points of maxima in their respective variable, thus being unhelpful in the cost function's minimization. We postulate it to be safe to ignore the leading sine/cosine terms when calculating the derivative, as they slow down the minimization in the best case, and actively interfere and cause false results in the worst-case. Formally, we say that

$$\frac{\partial \mathcal{L}}{\partial \theta_b} \approx \sum_{\substack{\mathbf{j}=[i,j] \\ i < j}} \sin(\theta_b - \psi_{\mathbf{j}}) \cos(\lambda_{\mathbf{j}}) G_{\mathbf{j}}(\theta_b, \phi_b), \quad (30a)$$

$$\frac{\partial \mathcal{L}}{\partial \phi_b} \approx \sum_{\substack{\mathbf{j}=[i,j] \\ i < j}} \cos(\theta_b - \psi_{\mathbf{j}}) \cos(\lambda_{\mathbf{j}}) G_{\mathbf{j}}(\theta_b, \phi_b), \quad (30b)$$

are a sufficiently good approximation of the derivatives. In a case where  $\phi_b = 0^\circ$  or  $\phi_b = 90^\circ$  would minimize the cost function, they would also be roots in this new approximation.

#### 2) Planar arrays

If one is working with a planar sensor array (be it rectangular, concentric, or any other planar arrangement), it is easy to see that  $\lambda_{\mathbf{j}} = \lambda_{\mathbf{j}'} \forall \mathbf{j}, \mathbf{j}'$ , and therefore the  $\cos(\lambda_{\mathbf{j}})$  term in both Eqs. (29a) and (29b) can be treated as a constant and ignored.

### 3) Linear arrays

One useful consideration for the linear array case is cylindrical symmetry in its steering vector. Given a direction  $(\theta, \phi)$ , there exists another direction  $(\theta', 0)$  such that their perceived response are identical. It is easy to see that

$$\theta' = \arccos(\cos(\theta) \cos(\phi)), \quad (31)$$

achieves this result. In this scenario, we assume that  $\phi_b = 0$ , and the DoA estimation is reduced to a single variable, namely  $\theta_b$ .

Furthermore, the azimuth for all sensors is constant as well, and we can safely assume  $\psi_j = 0 \forall j$  (through a coordinate system rotation). Thus  $\sin(\theta_b)$  is independent of  $j$  and can be factored; not only that, but it will also be ignored, as it is related to the chosen coordinate system and a constant. With these assumptions and considerations in mind, we have

$$\frac{\partial \mathcal{L}}{\partial \theta_b} \approx \sum_{\substack{j=[i,j] \\ i < j}} G(\theta_b, 0, j). \quad (32)$$

### D. Minimization scheme

Being able to minimize the cost function in  $\sigma_k$  and  $\Theta_b$ , the global minimization scheme is through the following steps:

- 1) Get an initial estimate  $\Theta_{b,0}$ .
- 2) Use Algorithm 1 to calculate  $\sigma^\dagger$ .
- 3) Check if derivatives with respect to  $\theta_b$  and  $\phi_b$  are within a desired threshold:
  - a) If not, go back to step 2, with  $\theta_b$  and  $\phi_b$  updated (such as via the gradient descent method);
  - b) If yes, break, and return the estimated parameters.
- 4) Construct the NCM  $\mathbf{R}_\eta$  as in Eq. (11).

The active-inactive analysis on  $\sigma_k$  has to be repeated for each iteration of the minimization on  $\Theta_b$ , since for one direction the constraints may have to be active, but not for a different neighboring direction.

### E. Proposed model theoretical features

The proposed estimation method exhibits several noteworthy properties. Its main appeal is its ability to jointly estimate the NCM and an interfering source's DoA, improving signal enhancement performance. Other important features are its inherent broadband formulation (although applicable to narrowband signals), leveraging spectral information and improving robustness in reverberant or noisy conditions; its ability to estimate both azimuth and elevation angles; and its independence of a voice activation detector, common in NCM estimators.

The method's iterative identity naturally enables source tracking with the DoA being updated periodically, assuming

the source position does not vary too rapidly. However, this iterative approach introduces some limitations, such as susceptibility to local minima in the cost function, and possible computational demand, depending on number of required steps. Its current form also isn't suitable for multi-source tracking.

## IV. FILTERING AND BEAMFORMING

Given the observed signal  $\mathbf{y}[l, k]$  and the environmental information on the desired and interfering sources, a filter can be applied on  $\mathbf{y}[l, k]$ . This filter is built to yield the best estimate of the desired signal at the reference, while minimizing the undesired signals in some way.

To this end, a linear filter  $\mathbf{h}[l, k]$  is applied to the observed signal  $\mathbf{y}[l, k]$ , producing an estimate  $\tilde{x}[l, k]$  that best approximates the desired signal at reference. This filtering process is defined by

$$\begin{aligned} \tilde{x}[l, k] &\approx x_1[l, k] \\ &= \mathbf{h}^H[l, k] \mathbf{y}[l, k] \\ &= \mathbf{h}^H[l, k] \mathbf{d}[k] x_1[l, k] + \mathbf{h}^H[l, k] \mathbf{\eta}[l, k]. \end{aligned} \quad (33)$$

The desired signal non-distortion can be achieved through the constraint  $\mathbf{h}^H[l, k] \mathbf{d}[k] = 1$  (this being called the distortionless constraint); and the reduction of the residual noise  $\mathbf{h}^H \mathbf{\eta}$  can be done through either direct minimization or with additional constraints. Based on this framework, several beamformers can be designed, each utilizing different information about the signals and environment, and aiming for distinct optimization goals.

### A. Full-framework outline

A diagram that presents the proposed technique's flowchart is in Fig. 2. Necessary input information is in blue, the minimization scheme — a simplification from Section III — in yellow, the filtering process (with any beamformer that exploits the obtained NCM and/or DoA estimations) in red, and the output information in green. Input information flow is shown in dashed lines, internal logic flow in dotted lines, and output flow in solid lines.

### B. NCM+DoA exploiting filters

To exploit both NCM and DoA estimations obtained via Section III, the linearly-constrained minimum variance (LCMV) beamformer can be used [24]. In addition to the distortionless constraint, it allows the placement of beampattern nulls in directions of known interference. In our case, we aim to use the interfering source's estimated DoA  $\Theta_b^*$  and its steering vector  $\mathbf{b}[k]$  to cancel  $\mathbf{p}[l, k]$ , the directional portion

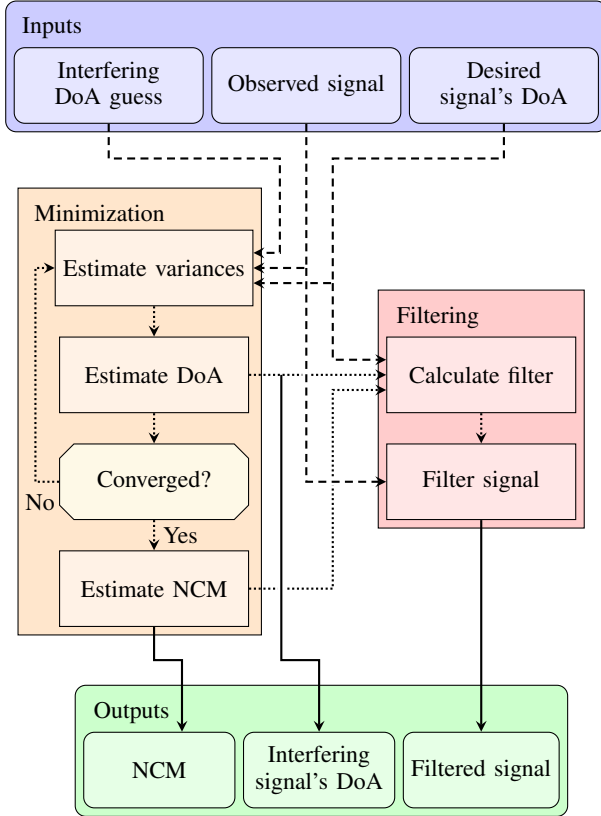


Fig. 2: Proposed NCM-DoA estimation technique + filtering scheme flowchart.

of the interfering signal  $\mathbf{n}[l, k]$ . For this, we define  $\mathbf{C}[k]$  as a  $M \times 2$  concatenation matrix,

$$\mathbf{C} = [\mathbf{d}, \mathbf{b}], \quad (34)$$

and the LCMV beamformer  $\mathbf{h}_{\text{LCMV}}[k]$  is given by

$$\mathbf{h}_{\text{LCMV}} = \mathbf{R}_{\tilde{\eta}}^{-1} \mathbf{C} \left[ \mathbf{C}^H \mathbf{R}_{\tilde{\eta}}^{-1} \mathbf{C} \right]^{-1} \mathbf{i}, \quad (35)$$

with  $\mathbf{i} = [1, 0]^T$ .

An alternative approach that only partially utilizes the estimated information is the minimum-variance distortionless response (MVDR) beamformer [24], which preserves the desired signal while minimizing the global noise. The standard MVDR formulation for the beamformer, denoted  $\mathbf{h}_{\text{MVDR}}[k]$ , is

$$\mathbf{h}_{\text{MVDR}} = \frac{\mathbf{R}_{\tilde{\eta}} \mathbf{d}}{\mathbf{d}^H \mathbf{R}_{\tilde{\eta}} \mathbf{d}}. \quad (36)$$

This beamformer is the same as explored in [20], but its necessary NCM is the obtained through the proposed (improved) methodology, instead of the original one.

### C. Literature-ready filter

A final option is adapting the LCMV beamformer to utilize the observed signal's CM  $\mathbf{R}_y$  instead of the estimated NCM

TABLE I: Simulation parameters, totaling 1458 configurations in total.

Parameter	Possible values		
$T_{60}$	0ms	500ms	800ms
$d_x$	50cm	150cm	300cm
$d_p$	50cm	150cm	300cm
SIR	-10dB	0dB	5dB
SCR	0dB	5dB	10dB
$\theta_b$	$10^\circ$	$30^\circ$	$50^\circ$
	$70^\circ$	$90^\circ$	$110^\circ$

$\mathbf{R}_{\tilde{\eta}}$ ; this being the Linearly-Constrained Minimum Power (LCMP) beamformer [25]. It is defined as

$$\mathbf{h}_{\text{LCMP}} = \mathbf{R}_y^{-1} \mathbf{C} \left[ \mathbf{C}^H \mathbf{R}_y^{-1} \mathbf{C} \right]^{-1} \mathbf{i}. \quad (37)$$

Since the LCMP beamformer uses the observed signal's CM — which can be estimated directly from the data — it is compatible with external DoA estimation methods, such as MUSIC [26]. While in ideal conditions the LCMV and LCMP beamformers are strictly equivalent, it is known that LCMP designs are more sensitive to steering errors [25] and can lead to distortion on the desired signal.

## V. SIMULATIONS

In this section, we present the different simulated acoustic scenarios, and compare the proposed model to the literature. This comparison will first analyze the DoA estimation, and later the filtering process.

### A. Scenarios: sources, receivers and environment

Simulated scenarios were used, considering a anechoic or slightly reverberant  $5\text{m} \times 6\text{m} \times 3\text{m}$  room. The sensor array's center is an uniform rectangular array with 16 sensors in a  $4 \times 4$  grid, with intersensor distance of  $\delta = 2\text{cm}$  in both directions, centered at  $(1.5\text{m}, 1.5\text{m}, 1\text{m})$ . The array's center is the origin for the environment's coordinate system. Nonetheless, for simplicity the estimation process' measurements (sensor-to-sensor angles and distances, and estimated DoA) are relative to the reference sensor.

All sources are positioned at  $0^\circ$  elevation — lying in the array's horizontal plane — and therefore only  $\theta_b$  needs to be estimated. The desired source's azimuth is fixed at  $\theta_d = 0^\circ$ , and the correlated sources are positioned 1m away from the origin, being 8 sources uniformly distributed in a circle. The approximations from Section III-C were also taken.

The reverberation time  $T_{60}$ , desired and interfering sources' distances  $d_x$  and  $d_p$  (relative to the sensor array's center), the interfering source's azimuth  $\theta_b$ , as well as Signal-to-Interference Ratio (SIR) and Signal-to-Correlated Ratio (SCR) are given in Table I, totaling  $6 \cdot 3^5 = 1458$  parameter

combinations. Signal power ratios are calculated between the desired signal's direct path component, and the respective reverberant contaminating signal. These possible parameter values were chosen to sweep a wide range of conditions, covering optimal and sub-optimal scenarios for both DoA estimation and filtering outcome.

The desired, interfering, and correlated sources' signals are respectively a male and female voice, and music excerpts; these being obtained from the SMARD database [27]. The room impulse responses (RIRs) between the sources and sensors were generated using Habets' RIR generator [28], [29], where the sources and sensors are assumed to be omnidirectional. All signals and RIRs used were resampled to 16kHz, and the time-frequency signals are obtained through the STFT, with  $K = 64$  bins, and Hamming windows with 50% overlap. The regularization parameter  $\epsilon$  (Eq. (10)) is set to 0.0001, to ensure that a minimal white noise is considered.

### 1) Benchmark algorithm

The proposed DoA estimation method will be compared to the traditional MUSIC algorithm [26]. For the MUSIC implementation, the angular search space was discretized using an exhaustive search with a fineness of  $1^\circ$ . To define a challenging test case, a scenario with a single dominant interfering source was simulated. The interferer's estimated DoA was determined by selecting the largest spectral peak from the MUSIC pseudospectrum, provided its angular separation was at least  $5^\circ$  from the (assumed known) desired source's direction.

The MUSIC algorithm is commonly used for narrowband DoA estimation, although extensions to broadband have been proposed [30]. For simplicity, we will apply it to each frequency bin, and employ two phasor-based averaging methods to obtain an angle estimate  $\bar{\theta}$ :

MUSIC: In the first one, a simple average will be taken across frequency, such that

$$\bar{\theta}_{\text{MUSIC}} = \angle \sum_k e^{j\theta_{\text{MUSIC}}[k]}. \quad (38)$$

wMUSIC: In the second one, a weighted average will be taken, weighing each bin by its MUSIC-estimated spectrum  $p_{\text{wMUSIC}}[k]$ , such that

$$\bar{\theta}_{\text{wMUSIC}} = \angle \sum_k p_{\text{wMUSIC}}[k] e^{j\theta_{\text{wMUSIC}}[k]}. \quad (39)$$

## B. Simulations for DoA estimation

For the proposed DoA estimator, the initial guess is always  $10^\circ$ – $15^\circ$  away from the true source, emulating a spread-out multi-initialization process or a reasonable previous time's estimate.

### 1) Evaluation criteria

To compare the DoA estimation processes, we calculate the angular error between the estimate (through any of the shown methods) and the true interfering signal's direction. This angular error is defined by

$$\Delta\theta_{b;\mathcal{C}} = \arccos \left( \hat{\mathbf{u}}_{\theta_b;\mathcal{C}} \cdot \hat{\mathbf{u}}_{\theta_b^*;\mathcal{C}} \right), \quad (40)$$

wherein  $\mathcal{C}$  denotes any of the 1458 possible configurations of parameters as presented in Table I, and  $\hat{\mathbf{u}}_{\theta_b;\mathcal{C}}$  is a unit vector with direction  $\theta_b$ , similarly for  $\hat{\mathbf{u}}_{\theta_b^*;\mathcal{C}}$ . Given a parameter (among those in the first column of Table I) and a value within the possible ones for this parameter, the results' statistics will be presented as boxplots (showing median, interquartile range and 9-th and 91-th percentiles) where the value is fixed and we marginalize over all other parameters, with each possible parameter being represented in a different subfigure. This enables the partition of each parameter's effects, and to compare among the chosen values of each.

### 2) Results and discussion

In this subsection, the proposed DoA estimator is compared to the standard average and weighted average MUSIC algorithms [26], for all configurations given in Table I.

#### a) Per-parameter analysis

The results in Fig. 3 present the DoA estimation error for the three presented approaches (proposed, standard average MUSIC, weighted average MUSIC), with each subfigure dissecting the performance along each parameter. The proposed method is denoted NCM (red), the standard MUSIC MSC (green, dashed), and the weighted MUSIC is denoted wMUSIC (in blue, dash-dotted). The box plots illustrate the error distributions for each method, grouped by each value for each parameter. Given the extensive range of angle errors, and the high concentration at smaller angles, the angular error is presented on a logarithmic scale.

Across all plots, the proposed technique consistently resulted in better DoA estimations, both in terms of median behavior as well as best- and worst-case outcomes (represented by the whiskers), mostly achieving errors below  $5^\circ$ . The MUSIC-based DoA estimation errors are frequently 2–3 times greater than the ones obtained through the proposed NCM-based approach.

Diving into the results for each fixed parameter, one sees that the DoA techniques' performance is most affected by  $T_{60}$ , SIR, and true  $\theta_b$  (respectively, Figs. 3a, 3d and 3f). It is expected that both a higher SIR (meaning the interfering signal is less powerful) and a higher reverberation time would correlate to a higher DoA estimation error, since the directional signal to be estimated would be less present in the overall signal. We also see that the proposed technique is more robust to these parameters, with the error increasing less than that of the MUSIC-based methods.

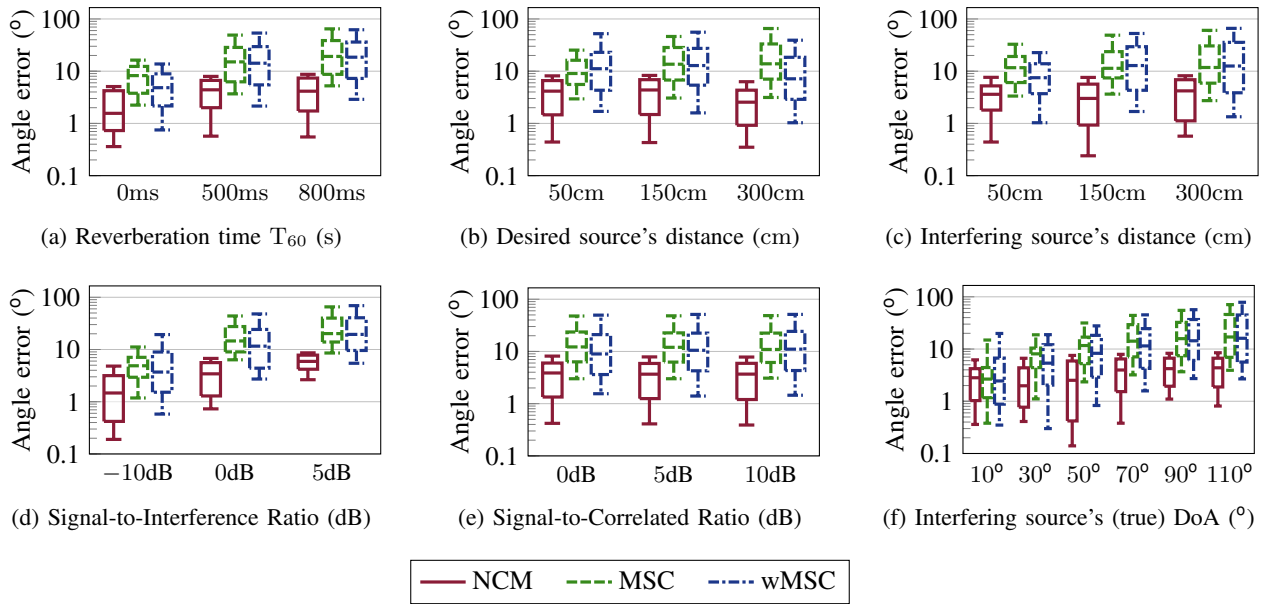


Fig. 3: Angle prediction error statistics (boxplots), for parameters in Table I.

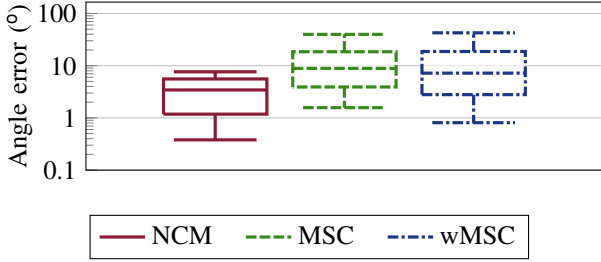


Fig. 4: Angle prediction error statistics (boxplots), for situations with invalid assumptions.

Interestingly, the proposed technique's performance is almost invariant with regards to the true DoA, with median performance fluctuating between 2-4°. Meanwhile, the MUSIC-based performance deteriorates as  $\theta_b$  increases, demonstrating the proposed technique's robustness to this parameter's variation.

As would be expected, parameters unrelated to the interfering source, such as the desired source's distance and input SCR, have little to no impact on the estimators' performance. Additionally, from Fig. 3(c) we see that the interfering source's distance to the array also has little impact on the outcome, with the proposed technique scoring similarly for all three presented values.

### b) Results under relaxed assumptions

Another class of scenarios that deserve some consideration are those where the assumptions from Section II aren't valid; namely, that the planar wave decomposition can't be applied, and that the coherent contaminating signals can't be modeled as an isotropic noise field. The violation of the aforementioned conditions applies when sources are close to the device, and/or

a low reverberation time is coupled to a high SCR. Results obtained for this conditions are presented in Fig. 4. It is seen that the proposed technique still works and outperforms the other methods.

### c) Discussion of general DoA estimation

Overall, we see a considerable robustness difference between the proposed technique and the broadband-adapted MUSIC ones, with the NCM-based method consistently resulting in more accurate DoA estimations for a wide range of parameter variations and conditions.

The proposed technique is also the top performer for an eccentric rectangular sensor array ( $8 \times 2$  rectangular array) and transposed directional sources' signals (desired female voice, and interfering male voice) conditions; both presented (along with the  $4 \times 4$  base-case) in Fig. 5, for a sub-set of parameters from Table I ( $d_x \in [150\text{cm}, 300\text{cm}]$ ,  $d_p \in [150\text{cm}, 300\text{cm}]$ ,  $\text{SIR} \in [-10\text{dB}, 0\text{dB}]$ ,  $\text{SCR} \in [0\text{dB}, 5\text{dB}]$ ;  $T_{60}$  and  $\theta_b$  unchanged), totaling 288 combinations. It is also noticeable that a male interfering source (more low frequency energy, harder to identify directionally), or a less symmetric array (has more accuracy in a preferred direction), both deteriorate the performance for all techniques, including the proposed one.

### C. Simulations for signal enhancement

The performance of the selected beamformers (Eqs. (35) to (37)) will be assessed for the scenarios given by the parameters in Table I, with a  $4 \times 4$  array, a male-voice desired signal, and a female-voice interfering signal; conditions identical to those originally analyzed in Paragraph (V-B2a).

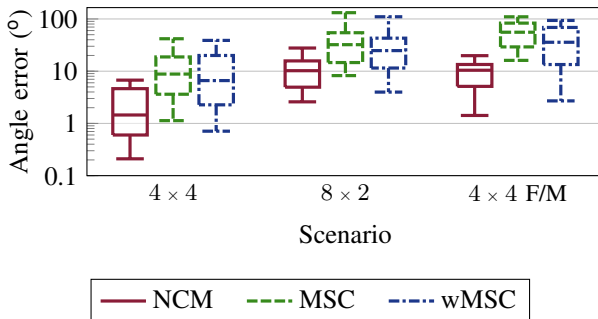


Fig. 5: Global angle prediction error statistics, for each considered situation (base case, eccentric array, and transposed voice types), with simplified parameter set.

### 1) Evaluation criteria

Different metrics are used to evaluate the performance of the selected beamformers (Eqs. (35) to (37)). For all metrics, we consider the desired signal as only the desired source signal's direct-path portion. All considered metrics are computed for the signals in the discrete time domain. The subscript  $(\cdot)_f$  denotes the filtered form of the respective signal; that is,  $x_f[l, k] = \mathbf{h}^H[l, k]\mathbf{x}[l, k]$ , and the same applies to all other filtered signals. For clarity, all metrics and their statistics will be presented on a logarithmic scale (dB).

To evaluate signal enhancement, the gains in SIR and SNR<sup>1</sup> (denoted gSIR and gSNR), and the interfering signal reduction factor (ISRF) will be used, these being respectively defined as

$$gSNR = \frac{\sigma_{x_f}^2 \sigma_{\eta_1}^2}{\sigma_{n_f}^2 \sigma_{x_1}^2}, \quad (41a)$$

$$gSIR = \frac{\sigma_{x_f}^2 \sigma_{\eta_1}^2}{\sigma_{n_f}^2 \sigma_{x_1}^2}, \quad (41b)$$

$$ISRF = \frac{\sigma_{p_1}^2}{\sigma_{p_f}^2}. \quad (41c)$$

While gSNR and gSIR measure the improvement in signal-to-contamination ratio, ISRF reflects the interfering source's signal direct-path rejection. Note that gSIR represents the (logarithmic) power-ratio between the observed signal's direct-path component, and the interfering signal  $n_1(t)$ , encompassing all of the latter's planar waves.

To characterize the desired signal's preservation, the desired signal reduction factor (DSRF)

$$DSRF = \frac{\sigma_{x_1}^2}{\sigma_{x_f}^2} \quad (42)$$

will be used. Although desired signal distortion index (DSDI) is also commonly used for assessing desired signal preservation, DSRF was chosen for its dB-friendly quality. We highlight that both DSRF and ISRF are measured w.r.t. the

<sup>1</sup>Here, SNR will represent the ratio w.r.t. the global noise  $\eta$ .

direct-path (or main planar wave) portion of the signals, disregarding reverberations and reflections.

Lastly, theoretical performance assessment is done through the broadband directivity factor (DF) and white-noise gain (WNG), defined as

$$DF = \frac{K}{\sum_{k=0}^K \mathbf{h}^H[k]\Gamma[k]\mathbf{h}[k]}, \quad (43a)$$

$$WNG = \frac{K}{\sum_{k=0}^K \mathbf{h}^H[k]\mathbf{h}[k]}, \quad (43b)$$

being  $\Gamma[k]$  the isotropic noise field pseudo-covariance matrix [22], [28]. These metrics estimate the beamformer's performance when exposed to an ideal isotropic noise field and a purely Gaussian noise, respectively.

The following three beamformers will be compared:

- LCMV: with proposed joint DoA and NCM estimation (red, solid line);
- MVDR: using only the modeled NCM (yellow, densely dotted);
- LCMP: using the conventional MUSIC algorithm (green, dashed);

Since both standard and weighted average MUSIC estimators had almost identical DoA error performance, we will present the results only the beamformer using the standard MUSIC algorithm, for simplicity.

### 2) Results and discussion

We present the boxplot results for each evaluation criterion and beamformer in Fig. 6, for the same simulated conditions given by the parameters in Table I. In the discussion, lower- and upper-bounds refer to the 9-th and 91-th whiskers; and lower- and upper-quartiles to the 25% and 75% quartiles.

#### a) Noise signal rejection

In terms of global noise rejection through the gSNR, we see that all techniques fared almost identically in terms of median outcome, with some differences in expected (quartiles) and extreme-case (whiskers) scenarios. A similar throughput was achieved in terms of gSIR, with all techniques achieving comparable results.

The first main difference can be seen in terms of interfering source's direct-path canceling, in which the proposed technique consistently outperformed the MUSIC one, and marginally the MVDR beamformer, in all boxplot measures. This is linked to the directional null present in the LCMV formulation, which isn't used in the MVDR. Interestingly, the MVDR had better direct-path interfering signal rejection than the LCMP, which also contain a null steering step in its beamformer.

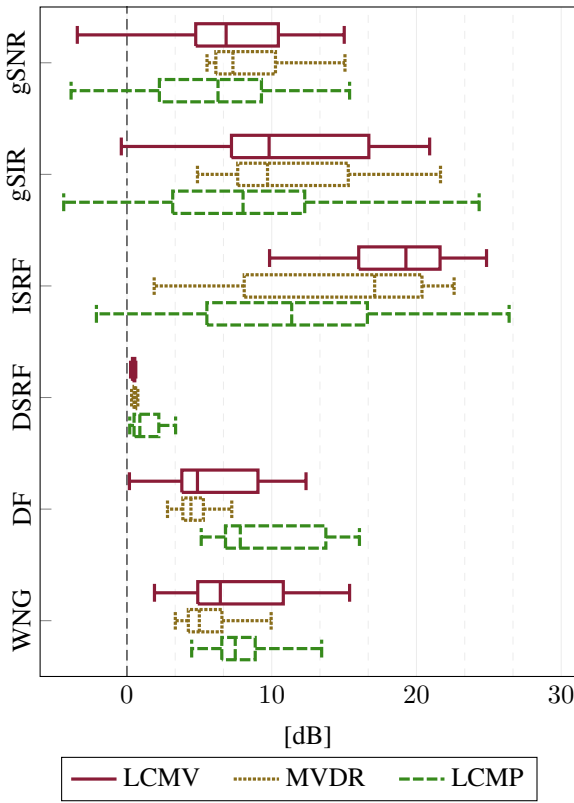


Fig. 6: Beamformers' performances, measured with different evaluation criteria (gSNR, gSIR, ISRF, DSRF, DF and WNG).

### b) Desired signal preservation

The DSRF results indicate that the NCM-based beamformers (yellow and red) exhibit significantly lower desired signal distortion compared to their MUSIC-based counterpart. This improvement is attributed to the proposed NCM design, which excludes the desired signal from the minimized covariance matrix, thus minimizing signal distortion. Both LCMV and MVDR beamformers resulted in practically identical distortions, with differences of less than 0.2dB between them. This desired signal distortion is also marginally linked to the slightly worse performance of the MUSIC beamformer in terms of gSNR and gSIR, as these gains can be defined based on signal reductions factors [31].

### c) Theoretical noise field metrics

In the directivity factor we see that the standard average MUSIC-based LCMP had a convincingly superior performance compared to the NCM-based beamformers, boxplot-available measurements. It also had better median, lower-quartile and lower-bound performance measured by WNG, although its upper-quartile and upper-bound scenarios were outmatched.

### d) Discussion on signal enhancement

Fig. 6 shows that all the proposed NCM-based beamformers have a very low desired signal reduction factor, this being directly correlated to the use of a NCM model, which excludes the desired signal from the covariance matrix to be used in filtering. The NCM-based LCMV beamformer also had a superior interfering source's direct-path rejection, which is expected, given the results as presented and discussed in Section V-B2.

All beamformers also performed comparably in the other two practical metrics. Meanwhile, the MSC-LCMP beamformer had the best performance in the theoretical measurements, widely for the DF, and marginally for the WNG.

## VI. CONCLUSION

In this paper, we introduced a joint estimation framework for the Noise Covariance Matrix (NCM) and Direction-of-Arrival (DoA) founded on a planar-wave decomposition and a broadband cost function. The proposed method built upon a previously proposed NCM model by incorporating a novel DoA estimator, which enables a more direct and efficient estimation pipeline; and by improving the foundational technique's mathematical framework, resulting in a quasi-linear solution (instead of an exhaustive search) for the NCM estimation portion of the problem. Qualities of the proposed approach include its iterative DoA search, broadband formulation, and independence of a voice activation detector.

Through detailed derivations and simulations, we showed that the method achieves accurate DoA estimates, especially for wider angle scenarios where conventional approaches often degrade. We also compared the proposed techniques to the literature in cases where our assumptions aren't valid, and for varying sensor array configurations and signal types, with the novel approach outperforming them in both scenarios.

We further applied the estimated parameters in beamforming, where the proposed model enabled superior interference suppression and desired signal preservation. Among all tested beamformers, the LCMV-based one (leveraging our proposed NCM and DoA estimates) consistently delivered the best overall performance across the featured signal enhancement metrics.

## REFERENCES

- [1] M. Wang, F. Gao, S. Jin, and H. Lin, "An Overview of Enhanced Massive MIMO With Array Signal Processing Techniques," *IEEE Journal of Selected Topics in Signal Processing*, vol. 13, no. 5, pp. 886–901, Sep. 2019.

- [2] T. Jansen, L. Hartog, D. Oetting, V. Hohmann, and H. Kayser, "Benefit of Hearing-Aid Amplification and Signal Enhancement for Speech Reception in Complex Listening Situations," *Trends in Hearing*, vol. 28, p. 23 312 165 241 271 407, Jan. 2024.
- [3] R. Haeb-Umbach et al., "Speech Processing for Digital Home Assistants: Combining Signal Processing With Deep-Learning Techniques," *IEEE Signal Processing Magazine*, vol. 36, no. 6, pp. 111–124, Nov. 2019.
- [4] A. Aubry, A. De Maio, and L. Pallotta, "A Geometric Approach to Covariance Matrix Estimation and its Applications to Radar Problems," *IEEE Transactions on Signal Processing*, vol. 66, no. 4, Feb. 15, 2018.
- [5] S. Salari, F. Chan, Y.-T. Chan, I.-M. Kim, and R. Cormier, "Joint DOA and Clutter Covariance Matrix Estimation in Compressive Sensing MIMO Radar," *IEEE Transactions on Aerospace and Electronic Systems*, vol. 55, no. 1, pp. 318–331, Feb. 2019.
- [6] C. Diouf, G. J. M. Janssen, H. Dun, T. Kazaz, and C. C. J. M. Tiberius, "A USRP-Based Testbed for Wideband Ranging and Positioning Signal Acquisition," *IEEE Transactions on Instrumentation and Measurement*, vol. 70, pp. 1–15, 2021.
- [7] Tuan Do-Hong and P. Russer, "Signal processing for wideband array applications," *IEEE Microwave Magazine*, vol. 5, no. 1, pp. 57–67, Mar. 2004.
- [8] P. Gaydecki, "A real time programmable digital filter for biomedical signal enhancement incorporating a high-level design interface," *Physiological Measurement*, vol. 21, no. 1, pp. 187–196, Feb. 1, 2000.
- [9] S. M. Qaisar, *Advances in Non-Invasive Biomedical Signal Sensing and Processing with Machine Learning*, 1st ed. Cham: Springer International Publishing AG, 2023.
- [10] A. M. Zoubir, V. Koivunen, Y. Chakhchoukh, and M. Muma, "Robust Estimation in Signal Processing: A Tutorial-Style Treatment of Fundamental Concepts," *IEEE Signal Processing Magazine*, vol. 29, no. 4, pp. 61–80, Jul. 2012.
- [11] J. Duník, O. Straka, O. Kost, and J. Havlík, "Noise covariance matrices in state-space models: A survey and comparison of estimation methods—Part I," *International Journal of Adaptive Control and Signal Processing*, vol. 31, no. 11, pp. 1505–1543, Nov. 2017.
- [12] M. Muhammad, M. Li, Q. Abbasi, C. Goh, and M. A. Imran, "A Covariance Matrix Reconstruction Approach for Single Snapshot Direction of Arrival Estimation," *Sensors*, vol. 22, no. 8, p. 3096, Apr. 18, 2022.
- [13] S. Greš, M. Döhler, V. K. Dertimanis, and E. N. Chatzi, "Subspace-based noise covariance estimation for Kalman filter in virtual sensing applications," *Mechanical Systems and Signal Processing*, vol. 222, p. 111 772, Jan. 2025.
- [14] M. Esfandiari and S. A. Vorobyov, "Noise Covariance Matrix Estimation in Block-Correlated Noise Field for Direction Finding," *IEEE Signal Processing Letters*, vol. 32, pp. 531–535, 2025.
- [15] U. Kjems and J. Jensen, "Maximum likelihood based noise covariance matrix estimation for multi-microphone speech enhancement," *2012 Proceedings of the 20th European Signal Processing Conference*, pp. 295–299, 2012.
- [16] J. Duník, O. Straka, and M. Simandl, "On Autocovariance Least-Squares Method for Noise Covariance Matrices Estimation," *IEEE Transactions on Automatic Control*, vol. 62, no. 2, pp. 967–972, Feb. 2017.
- [17] A. Barthelme and W. Utschick, "DoA Estimation Using Neural Network-Based Covariance Matrix Reconstruction," *IEEE Signal Processing Letters*, vol. 28, 2021.
- [18] C. Stöckle, J. Munir, A. Mezghan, and J. A. Nossek, "DoA Estimation Performance and Computational Complexity of Subspace- and Compressed Sensing-based Methods," *19th International ITG Workshop on Smart Antennas*, pp. 1–6, 2015.
- [19] F. Yan, M. Jin, and X. Qiao, "Low-Complexity DOA Estimation Based on Compressed MUSIC and Its Performance Analysis," *IEEE Transactions on Signal Processing*, vol. 61, no. 8, pp. 1915–1930, Apr. 2013.
- [20] A. H. Moore, S. Hafezi, R. R. Vos, P. A. Naylor, and M. Brookes, "A Compact Noise Covariance Matrix Model for MVDR Beamforming," *IEEE/ACM Transactions on Audio, Speech, and Language Processing*, vol. 30, pp. 2049–2061, 2022.
- [21] O. Yilmaz and S. Rickard, "Blind Separation of Speech Mixtures via Time-Frequency Masking," *IEEE Transactions on Signal Processing*, vol. 52, no. 7, pp. 1830–1847, Jul. 2004.
- [22] N. Epain and C. T. Jin, "Spherical Harmonic Signal Covariance and Sound Field Diffuseness," *IEEE/ACM Transactions on Audio, Speech, and Language Processing*, vol. 24, no. 10, pp. 1796–1807, Oct. 2016.
- [23] R. T. Rockafellar, "Lagrange Multipliers and Optimality," *SIAM Review*, vol. 35, no. 2, pp. 183–238, Jun. 1993.
- [24] M. Souden, J. Benesty, and S. Affes, "A Study of the LCMV and MVDR Noise Reduction Filters," *IEEE Transactions on Signal Processing*, vol. 58, no. 9, pp. 4925–4935, Sep. 2010.
- [25] P. Vergallo et al., "Processing EEG signals through beamforming techniques for seizure diagnosis," in *2012 Sixth International Conference on Sensing Technology (ICST)*, Kolkata: IEEE, Dec. 2012, pp. 497–501.
- [26] P. Gupta and S. Kar, "Music and improved music algorithm to estimate direction of arrival," in *2015 International Conference on Communications and Signal Processing (ICCP)*, 2015, pp. 0757–0761.
- [27] J. K. Nielsen, J. R. Jensen, S. H. Jensen, and M. G. Christensen, "The single- and multichannel audio recordings database (SMARD)," in *2014 14th International Workshop on Acoustic Signal Enhancement (IWAENC)*, Juan-les-Pins: IEEE, Sep. 2014, pp. 40–44.
- [28] E. A. P. Habets and S. Gannot, "Generating sensor signals in isotropic noise fields," *The Journal of the Acoustical Society of America*, vol. 122, no. 6, pp. 3464–3470, Dec. 1, 2007.

- [29] E. Habets, *Room Impulse Response Generator*, version v2.1, 2020.
- [30] M. A. Alrmah, S. Weiss, and S. Lambotharan, “An extension of the MUSIC algorithm to broadband scenarios using a polynomial eigenvalue decomposition,” *2011 19th European Signal Processing Conference*, pp. 629–633, 2011.
- [31] J. Benesty, I. Cohen, and J. Chen, *Fundamentals of signal enhancement and array signal processing*. John Wiley & Sons, 2017.

## APPENDIX

### A. Proofs and Theorems

Let the function  $F(\boldsymbol{\sigma}) \equiv F(\mathbf{R}_{\tilde{\mathbf{y}}}(\boldsymbol{\sigma}_k, \Theta))[k]$  from Eq. (12) be the function to be minimized w.r.t.  $\boldsymbol{\sigma}$ , under  $\boldsymbol{\sigma} \geq \mathbf{0}$ .

Given that  $F(\boldsymbol{\sigma})$  is quadratic on any element of  $\boldsymbol{\sigma}$  (obtainable from Eq. (14)), it is guaranteed to have a global extrema, denoted  $\boldsymbol{\sigma}^*$ , which may not respect the constraints. Since  $F(\boldsymbol{\sigma})$  is the sum of squared real numbers, its extrema is a minimum. Given the triviality of scenarios where  $\boldsymbol{\sigma}^* \geq \mathbf{0}$ , we assume that  $\boldsymbol{\sigma}^* \not\succeq \mathbf{0}$ , having at least one negative entry. We let  $\boldsymbol{\sigma}^\dagger$  be the minimum of  $F(\boldsymbol{\sigma})$  which fulfills  $\boldsymbol{\sigma}^\dagger \geq \mathbf{0}$ ; and define  $\boldsymbol{\sigma}(t) = \boldsymbol{\sigma}^* + (\boldsymbol{\sigma}^\dagger - \boldsymbol{\sigma}^*)t$  as a solution parameterized by  $t$ ; trivially,  $\boldsymbol{\sigma}(0) = \boldsymbol{\sigma}^*$ , and  $\boldsymbol{\sigma}(1) = \boldsymbol{\sigma}^\dagger$ . We also define  $J(t) \equiv F(\boldsymbol{\sigma}^* + (\boldsymbol{\sigma}^\dagger - \boldsymbol{\sigma}^*)t)$ .

**Theorem 1.** *If the global minimum isn't in the feasible region, the constrained minimum lies in its boundary.*

We assume that  $\boldsymbol{\sigma}^\dagger > \mathbf{0}$ , strictly greater; that is, the constrained minimum isn't on the boundary where some entries are 0. Through the intermediate value theorem, there exists some  $t' \in [0, 1]$  for which  $t \geq t'$  implies that  $\boldsymbol{\sigma}(t) \geq \mathbf{0}$  (greater or equal).

Using  $J(t)$  as defined previously using the definition from Eq. (14), replacing  $\boldsymbol{\sigma} = \boldsymbol{\sigma}^* + (\boldsymbol{\sigma}^\dagger - \boldsymbol{\sigma}^*)t$ , and expanding, leads to

$$\begin{aligned} J(t) &= \sum_{\mathbf{j}} \left| \left[ \sum_{z \in [x, u, \gamma, v]} R_{\mathbf{z}; \mathbf{j}} \sigma_z(t) \right] - R_{\mathbf{y}, \epsilon; \mathbf{j}} \right|^2 \\ &= \sum_{\mathbf{j}} (a_{\mathbf{j}}^{\mathbb{R}} t - b_{\mathbf{j}}^{\mathbb{R}})^2 + (a_{\mathbf{j}}^{\mathbb{I}} t - b_{\mathbf{j}}^{\mathbb{I}})^2 \\ &= At^2 + Bt + C, \end{aligned} \quad (\text{A.1})$$

with

$$A = \sum_{\mathbf{j}} |a_{\mathbf{j}}|^2, \quad (\text{A.2a})$$

$$B = -2 \sum_{\mathbf{j}} a_{\mathbf{j}}^{\mathbb{R}} b_{\mathbf{j}}^{\mathbb{R}} + a_{\mathbf{j}}^{\mathbb{I}} b_{\mathbf{j}}^{\mathbb{I}}, \quad (\text{A.2b})$$

$$C = \sum_{\mathbf{j}} |b_{\mathbf{j}}|^2, \quad (\text{A.2c})$$

$$a_{\mathbf{j}} = \sum_{z \in [x, u, \gamma, v]} R_{\mathbf{z}; \mathbf{j}} (\sigma_z^\dagger - \sigma_z^*), \quad (\text{A.2d})$$

$$b_{\mathbf{j}} = R_{\mathbf{y}, \epsilon; \mathbf{j}} + \sum_{z \in [x, u, \gamma, v]} R_{\mathbf{z}; \mathbf{j}} (\sigma_z^\dagger). \quad (\text{A.2e})$$

Note that  $A > 0$ , indicating that  $J(t)$  is a positively-curved quadratic function in  $t$ . By definition,  $J(0)$  minimizes the function, so  $J(t) \geq J(0) \forall t$ , and in particular  $\forall t \in [0, 1]$ . Since  $J'(t)_{t=0} = 0$ , we also have that  $B = 0$ . So, for any  $0 < t' \leq t$

$$\begin{aligned} J(t') &= A(t')^2 + C \\ &< At^2 + C = J(t), \end{aligned} \quad (\text{A.3})$$

Since  $t'$  is the smallest value for which  $J(t') \geq 0$ , and  $t' < 1$ , then  $J(t') < J(1) = \boldsymbol{\sigma}^\dagger$ , contradicting the premise that  $\boldsymbol{\sigma}^\dagger$  is the optimal solution within our constraint space. Therefore,  $\boldsymbol{\sigma}^\dagger \not\succeq \mathbf{0}$ , and the optimal solution has (at least) one zero entry.  $\blacksquare$

**Theorem 2.** *The constrained entries of  $\boldsymbol{\sigma}^\dagger$  are at most the negative entries of  $\boldsymbol{\sigma}^*$ .*

Since  $\boldsymbol{\sigma}^\dagger \geq \mathbf{0}$ , and  $\boldsymbol{\sigma}(t)$  is linear in  $t$ , the entries of  $\boldsymbol{\sigma}^*$  which are greater than 0 will be positive  $\forall t$ . This implies that any positive entry of  $\boldsymbol{\sigma}(0) = \boldsymbol{\sigma}^*$  will need not be constrained in the search for  $\boldsymbol{\sigma}(1) = \boldsymbol{\sigma}^\dagger$ , being strictly positive along the curve defined by  $\boldsymbol{\sigma}(t)$ ,  $t \in [0, 1]$ . This, along with Theorem 1, implies that only the negative entries of  $\boldsymbol{\sigma}^*$  may have active constraints.

We remark that not all negative entries  $\boldsymbol{\sigma}^*$  must be set to 0. Each constraint added changes the matrix  $\mathbf{A}[k]$  from Eqs. (22a) and (23), changing the manifold over which the minimization is done, and resulting in a different minimum where the other negative entries of  $\boldsymbol{\sigma}^*$  may be naturally positive.  $\blacksquare$